

Article

# Francis Turbine Blade Design on the Basis of Port Area and Loss Analysis

Zhenmu Chen <sup>1</sup>, Patrick M. Singh <sup>1</sup> and Young-Do Choi <sup>2,\*</sup>

<sup>1</sup> Graduate School, Department of Mechanical Engineering, Mokpo National University, Mokpo, Jeollanam-do 58555, Korea; chenchenmu@163.com (Z.C.); pms72006@yahoo.com (P.M.S.)

<sup>2</sup> Department of Mechanical Engineering, Institute of New and Renewable Energy Technology Research, Mokpo National University, Mokpo, Jeollanam-do 58555, Korea

\* Correspondence: ydchoi@mokpo.ac.kr; Tel.: +82-61-450-2419

Academic Editor: Jang-Ho Lee

Received: 17 December 2015; Accepted: 1 March 2016; Published: 4 March 2016

**Abstract:** In this study, a Francis turbine with specific speed of 130 m-kW was designed on the basis of the port area and loss analysis. The meridional shape of the runner was designed focusing mainly on the combination of the guide vane loss analysis and experience. The runner blade inlet and outlet angles were designed by calculation of Euler's head, while the port area of blade was modified by keeping constant angles of the blade at inlet and outlet. The results show that the effect of the port area of runner blade on the flow exit angle from runner passage is significant. A correct flow exit angle reduces the energy loss at the draft tube, thereby improving the efficiency of the turbine. The best efficiency of 92.6% is achieved by this method, which is also similar to the design conditions by the one dimension loss analysis.

**Keywords:** Francis turbine; runner design; port area; performance; loss analysis

## 1. Introduction

There is an increasing demand for renewable energy for sustainable development to solve the coming energy crisis. The necessity of the use of renewable energy as one of the clean and sustainable natural energy resources has become high. Francis turbines are applicable to a wide range of head and specific speed values. Their wide range of applicability and easier structural design makes Francis turbines more advantageous than other hydraulic turbines. As a key component of a Francis turbine facility, the runner performance plays a vital role in the performance of the turbine. A Francis turbine runner blade with good performance by the one dimensional hydraulic design method can be designed effectively and successfully. Korea relies on foreign products, and the technology for local manufacture was limited until 2010 [1]. Currently, Korea is in the process of developing its hydropower technology.

In this study, a new method on basis of the port area and loss analysis to design a Francis turbine runner was developed for the Miryang power station in Korea. In this study, the port area is defined as the minimum blade passage area at the exit of the blade passage, which will be defined in more detail in Section 2.2. The meridional shape of the runner was designed on the basis of the combination of the guide vane loss analysis and experience. The runner blade inlet and outlet angles were designed by calculation of Euler's head, and the port area of blade was modified by keeping the inlet and outlet angles of the blade constant. Unlike conventional direct design methods, where much attention is paid to draw the meridional plane streamlines to obtain the meridional velocity [2], the new method tries to adjust the port area of the runner blade passage to correct the outflow angle at the runner exit.

## 2. Turbine Runner Design and Numerical Method

Figure 1 shows the flow chart of the Francis turbine runner blade design. For one dimension hydraulic design, calculation is required for the blade angle at leading and trailing edges. For the meridional plane shape design part, because the guide vane is movable, a minimum guide vane loss exists according to different guide vane height ( $B_g$ ) at the design condition. In this study, the guide vane height is determined according to the guide vane loss analysis, and the other parameters, such as the runner inlet and outlet diameters, are determined by experience. The outflow angle from the runner passage is controlled by the runner port area and blade outlet angle. Moreover, the blade outlet angle can be calculated by the Euler head equation. Therefore, the port area can be determined by the outflow angle from the runner passage.

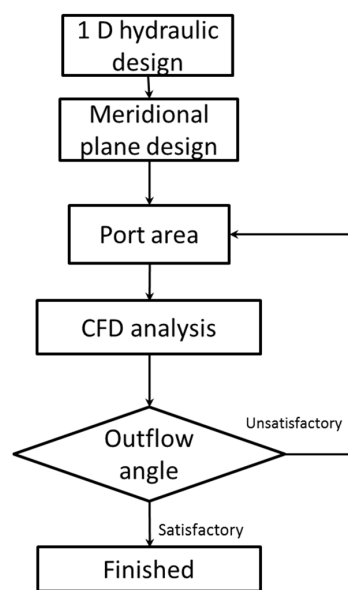


**Figure 1.** Flow chart of Francis turbine runner blade design. CFD: computational fluid dynamics.

### 2.1. One Dimension Loss Analysis

In this study, the runner is designed for the Miryang power station in Korea. The turbine design point is at  $H_e = 64.2$  m for the effective head, the  $Q = 1.21$  m<sup>3</sup>/s for flow rate and the rotational speed is  $N = 914$  min<sup>-1</sup>. The specific speed at the design point is  $N_s = 130$  m-kW, which is within the range of Francis turbines with  $N_s = 60$ –450 m-kW and  $H = 20$ –700 m [3].

To obtain the guide vane pressure loss coefficient for the meridional shape design, the numerical analysis was performed with different guide vane openings ( $a_0$ ) and heights ( $B_g$ ). The boundary condition at inlet was set as mass flow rate and the flow angle was set same as the guide vane inlet angle. Inlet turbulence condition was specified as 5% turbulence intensity. The boundary condition of average static pressure was set at outlet of the guide vane passage. According to the previous study [4,5], the SST  $k$ - $\omega$  turbulence model is adopted as turbulence model, which has been well known to estimate both separation and vortex occurrence on the wall of a complicated blade shape. Moreover, the value of  $y^+$ , which means non-dimensional distance from wall [6,7], is determined to be around 9 for the guide vane blade surface. The pressure difference measurement locations are shown in Figure 2. The location P2 is between the guide vane and stay vane, and location P3 is between the guide and runner vane.

For evaluating the guide vane pressure loss coefficient ( $\zeta$ ), the equation is determined by Equation (1):

$$\zeta = \frac{(p_2 - p_3) \times 2}{\rho V_{th}^2} \quad (1)$$

where  $p_2$  and  $p_3$  are the averaged total pressure at locations P2 and P3, respectively.  $V_{th}$  is the velocity at the throat of guide vane passage and  $\rho$  is the density of the water.

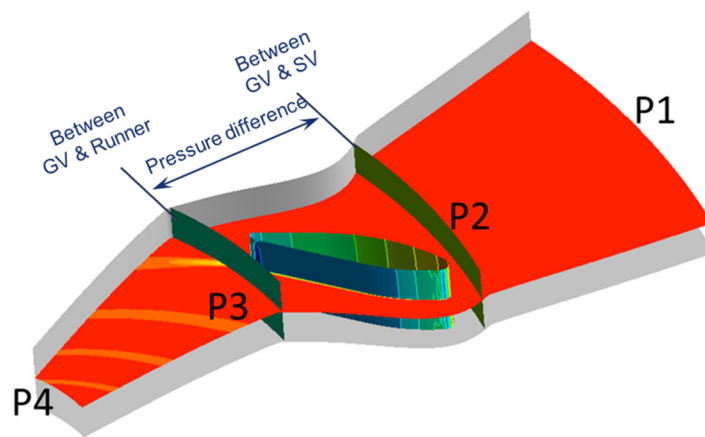


Figure 2. Pressure difference location for guide vane loss analysis.

The result of the guide vane flow angle according to the guide vane opening ratio ( $a_0/D_{r1}$ ) is shown in Figure 3. The flow angle is the measurement at the outlet of guide vane, which means the flow angle is the outflow angle of guide vane passage. The relationship between the outflow angle and guide vane opening ratio is obtained as shown in Figure 3.

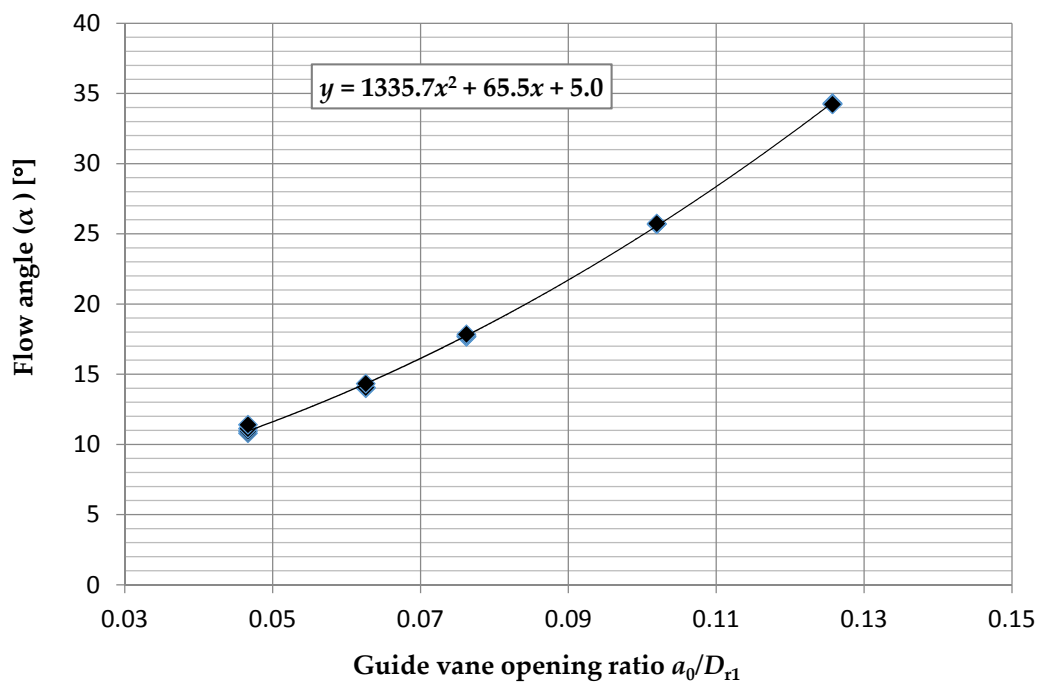


Figure 3. Relation of flow angle and guide vane opening ratio.

Figure 4 shows the relation of the pressure loss coefficient and guide vane hydraulic radius ratio ( $m/D_{r1}$ ). It can be seen that there is lower pressure loss coefficient at the larger guide vane hydraulic radius. Moreover, the relationship between pressure loss coefficient and guide vane hydraulic radius ratio can be obtained as shown in Figure 4. The definition of the hydraulic radius ( $m$ ) is shown in Equation (2):

$$m = \frac{a_0 B_g}{2 \times (a_0 + B_g)} \tag{2}$$

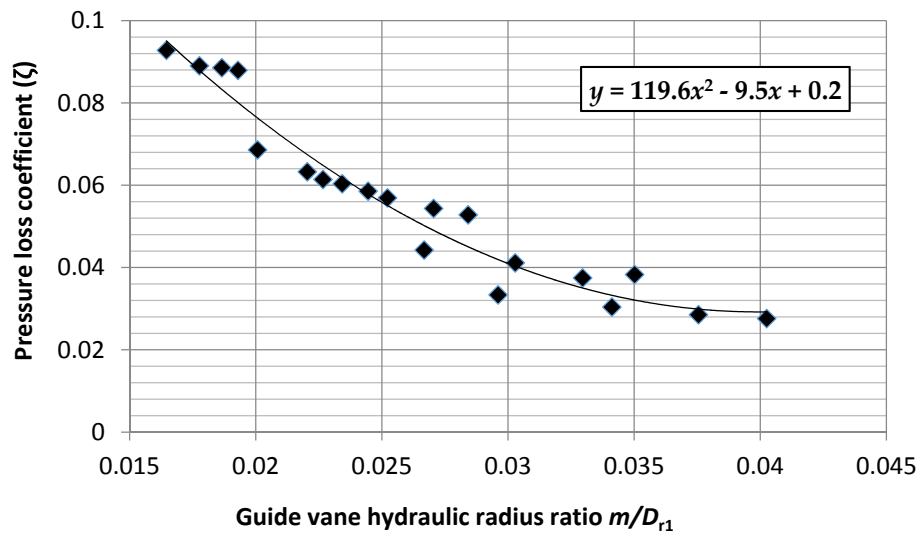


Figure 4. Relation of the pressure loss coefficient and guide vane hydraulic radius ratio.

For the design and best efficiency point, it can be assumed that there is no swirl flow remaining at the draft tube. Therefore, according to the Euler turbine head equation [2,8–11], the relation between Euler head, guide vane height ( $B_g$ ) and the outflow angle from guide vane passage ( $\alpha$ ) is shown in Equation (3). Additionally, according to the pressure loss coefficient, the relation between guide vane head loss, guide vane opening ( $a_0$ ) and guide vane height ( $B_g$ ) is derived as shown in Equation (4):

$$H_{th} = \frac{U_1 V_{u1}}{g} = \frac{1}{g} \left( \frac{NQ}{60B_g \tan \alpha} \right) \tag{3}$$

$$H_{gv} = \zeta \frac{V_{th}^2}{2g} = \zeta \frac{1}{2g} \left( \frac{Q}{Z_g a_0 B_g} \right)^2 \tag{4}$$

According to the outflow angle from guide vane passage, guide vane pressure loss coefficient and the Euler head, the one dimension loss analysis results are plotted in Figure 5. These results are obtained only at design flow rate and head. As the Euler turbine head for the design point is constant and the turbine head is controlled by the guide vane passage opening, the guide vane opening ratio ( $a_0/D_{r1}$ ) has to be determined for a specified guide vane height ( $B_g$ ), as shown in Figure 5.

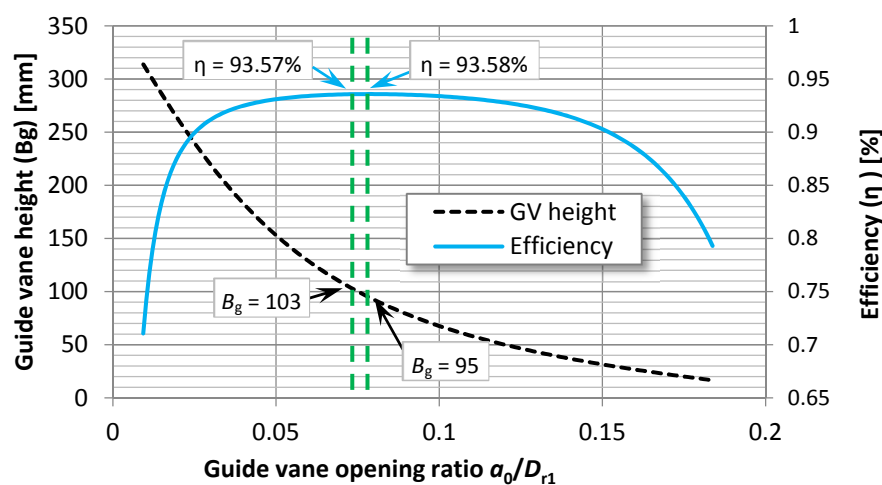
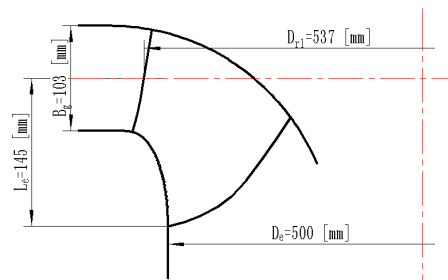


Figure 5. One dimension loss analysis result.

The efficiency curve shown in the graph is the design point efficiency with different designs of guide vane heights ( $B_g$ ) and guide vane opening ratios ( $a_0/D_{r1}$ ). As a result, it can be seen that there is a best efficiency point by the different guide vane opening ratio ( $a_0/D_{r1}$ ). Additionally, there is a relatively wide guide vane opening ratio (guide vane height) with high efficiency, meaning that there is a wide range for the design of guide vane opening ratio and guide vane height. In this study, in order to fit the runner to the existing Francis turbine plant for performance test, the guide vane height ( $B_g$ ) of 103 mm is selected, which belongs to the high efficiency range according to the one dimension loss analysis. Finally, the meridional plane shape with basic dimensions is determined as shown in Figure 6.



**Figure 6.** Meridional plane shape and basic dimensions.

## 2.2. Turbine Runner Blade Model

Figure 7 reveals the definition of the runner blade port area. The port area of the runner blade is located at the exit of the runner flow passage, which is the minimum area at the runner flow passage. Therefore, the dimension of the port area plays a very important role in controlling the exit relative velocity from runner passage as shown in Figure 8. The relative velocity ( $W_2$ ) reduces with increasing port area, which causes the outflow angle ( $\alpha_2$ ) to drop. The outflow angle from runner passage is perpendicular ( $90^\circ$ ) only with correct relative velocity. Therefore, it is possible to achieve correct outflow angle by modifying the port area and relative outflow velocity.

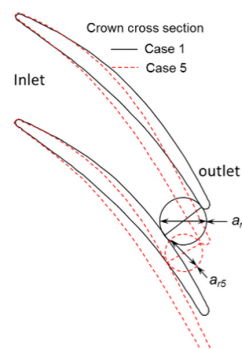


**Figure 7.** Definition of the runner blade port area.

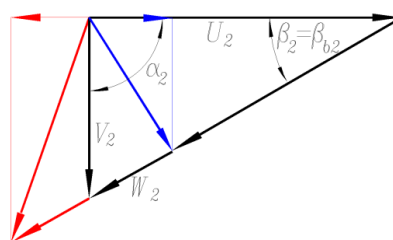


**Figure 8.** Velocity triangle at runner outlet.

Figure 9 shows the port area distribution from crown to shroud in the runner flow passage 1. The port area has to be modified until the outflow angle is satisfactory.

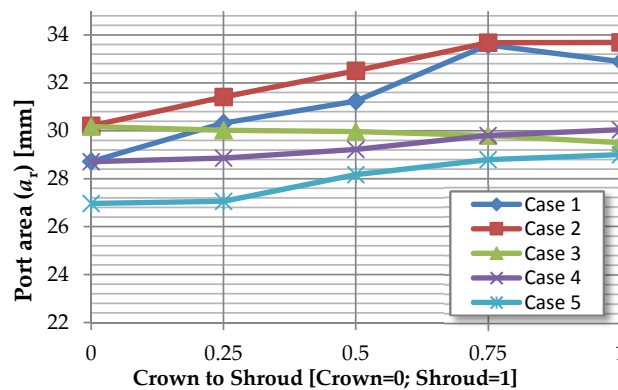


Figure 9. Port area distribution of the five cases.

### 2.3. Numerical Method

Computational fluid dynamics (CFD) analysis is a very useful tool for predicting hydro machinery performance at various operating conditions [12–15]. Commercial code of ANSYS CFX [16] was employed to predict the characteristics of the Francis turbine. The general connection was set as “stage” condition between the rotational area and the fixed area. The SST  $k-\omega$  model was selected for the turbulence model. Inlet turbulence condition is specified as 5% turbulence intensity and the flow direction is normal to the inlet boundary.

There are two kinds of numerical domain for the CFD analysis. Considering the computation time consumption, the cases for different port area calculation (Cases 1–5) was conducted by 1 pitch domain. Moreover, for the Francis turbine performance analysis, the full domain analysis was conducted. For 1 pitch flow passage (1 stay vane, 1 guide vane and 1 runner blade flow passage), the mass flow condition was applied at the inlet and the static pressure was set at the outlet of the calculation domain. However, for the full domain calculation, the total pressure boundary condition was applied at the inlet, and the static pressure was set at the outlet of the domain. This is done to maintain the design head and check the flow rate is matched with design point.

For 1 pitch flow passage, the total number of elements is  $5.5 \times 10^6$ , for which the  $y^+$  around the blade surface is 9. Therefore, the total number of elements for 1 pitch flow passage is sufficient for reliable results. In order to exclude the effect of mesh on the prediction accuracy, the mesh dependence was conducted for full domain CFD analysis as shown in Figure 10. The efficiency was normalized by the selected efficiency. It can be concluded that the turbine efficiency is insensitive after the number of elements exceed  $7.5 \times 10^6$ . Therefore, the number of elements around  $7.5 \times 10^6$  was selected for full domain calculation.

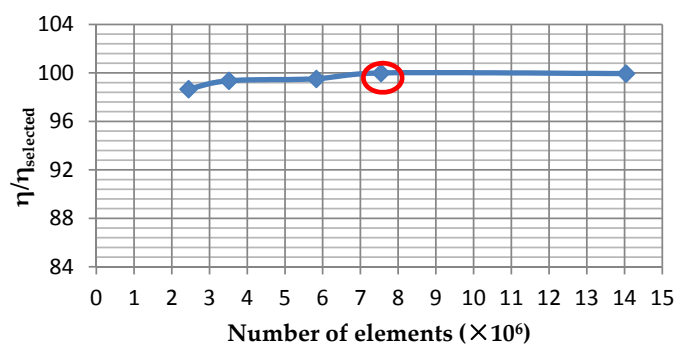


Figure 10. Mesh dependence for the full domain calculation.

### 3. Results and Discussion

#### 3.1. Outflow Pattern

The criterion for the runner blade port area design is the outflow angle. The effect of draft tube on recycling the kinetic energy is limited. Especially, the kinetic energy from the circumferential velocity is very hard to collect. Therefore, a correct outflow angle plays a role of reducing the loss at draft tube and improving the efficiency of the turbine. The modification of port area is satisfactory until the outflow angle is as close to  $90^\circ$ . Figure 11 shows the outflow angle distribution from runner crown to shroud. The outflow angle of Case 5 is located close to  $90^\circ$  with only small deviation. Moreover, as the effect of boundary wall, the deviation increases near the crown and shroud walls. Overall, the port area and the outflow angle of Case 5 are satisfactory for the runner design.

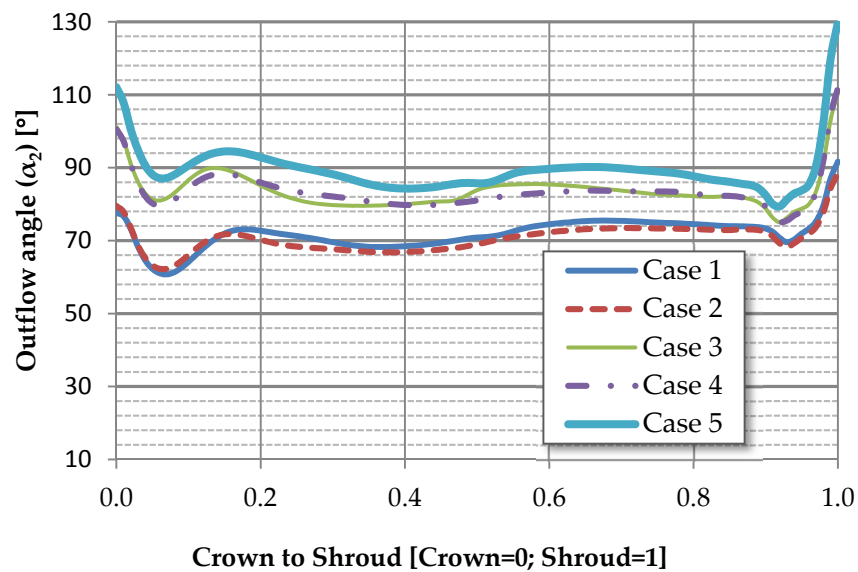


Figure 11. Outflow angle distribution.

Figure 12 shows the streamline distribution in the draft tube. It is clearly indicated that the streamline of Case 1 in the draft tube shows large swirl flow, which increases the loss at the draft tube. However, by modifying the port area to a correct extent (Case 5), there are vertically straight streamlines in the draft tube, and exit flow angle is close to  $90^\circ$ . The effect of modifying the port area on correcting the exit flow angle is significant in reducing the swirl flow.

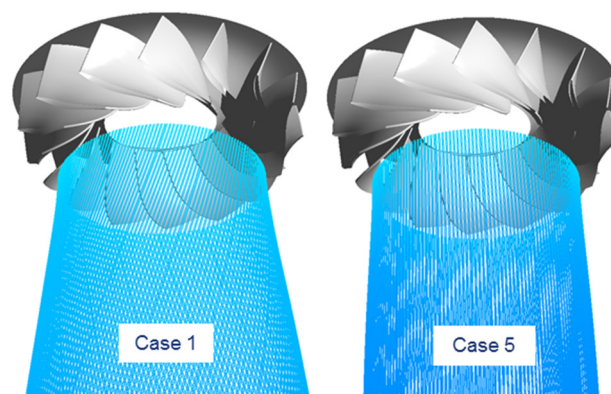


Figure 12. Streamline distribution in draft tube.

### 3.2. Loss Analysis

For the loss analysis, the equation is defined as following:

$$H_{\text{Loss}} = \frac{\Delta p_{\text{total}}}{\rho g} \quad (5)$$

$$H_{\text{Loss runner}} = \frac{\Delta p_{\text{total}} - \frac{T\omega}{Q}}{\rho g} \quad (6)$$

where the  $H_{\text{Loss}}$  is the pressure loss for the stay vane, guide vane and draft tube,  $H_{\text{Loss runner}}$  is the pressure loss for the runner passage.

Figure 13 shows the loss distribution on each component. As the result is obtained from 1 pitch analysis without casing, there is no casing component loss analysis. The loss exists to a large extent at draft tube at Cases 1 and 2, for which swirl flow exists with large deviation outflow angle from  $90^\circ$  (as shown in Figure 11). However, the loss at draft tube reduces with correct outflow angle. The total loss distribution by each case is obtained in Figure 14. There is minimum total loss at Case 5, which satisfies outflow angle from runner exit and has the lowest loss at draft tube.

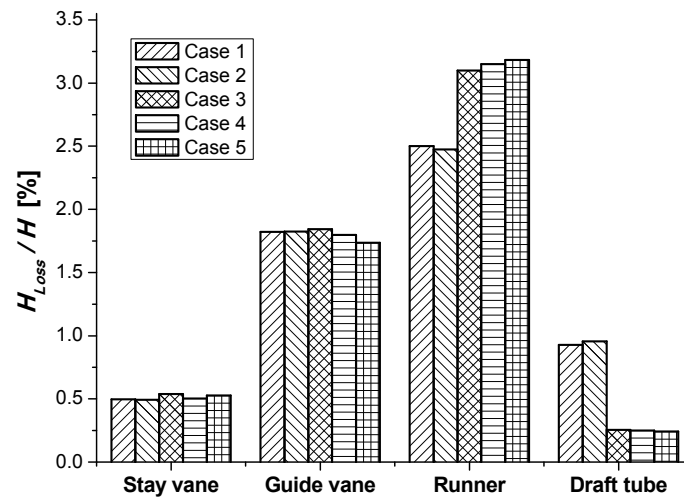


Figure 13. Loss distribution on each component.

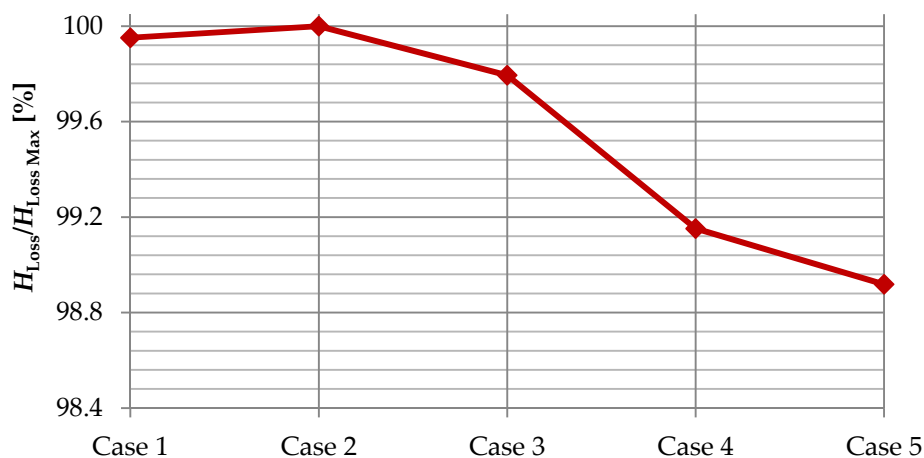


Figure 14. Total loss distribution by each case.

### 3.3. Performance Analysis

The performance analysis of the Francis turbine was conducted by full domain as shown in Figure 15. There is best efficiency point of 92.6% with leakage loss at the  $Q_{11}$  of 0.525, at which the flow rate is the design flow rate for this Francis turbine. In comparison to the efficiency without leakage, there is 1.4% difference at the design flow rate. The leakage loss of 1.4% consists of disk friction loss and volume loss.

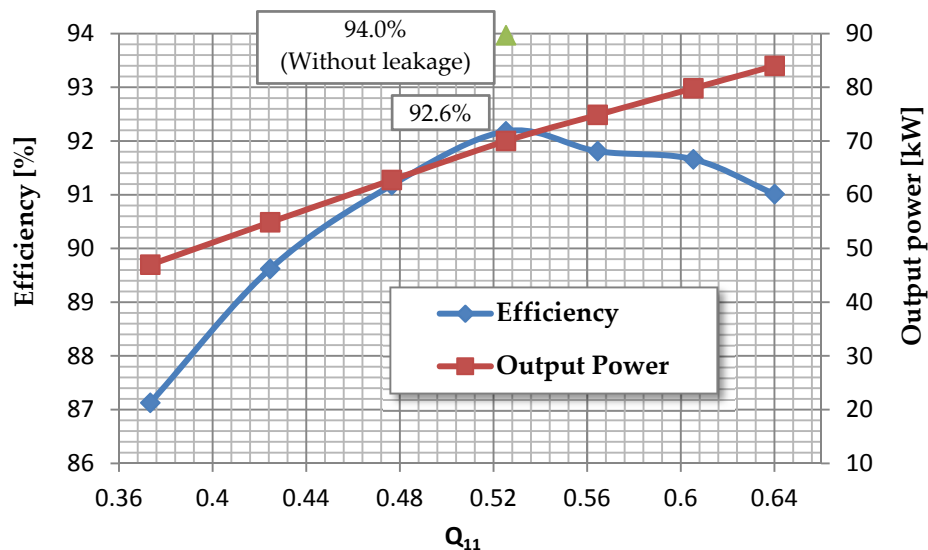


Figure 15. Performance of the Francis turbine by the flow rate.

Figure 16 shows the component loss at different flow rates. It can be seen that the loss at the casing and stay vane passage is relatively small and the loss increases slightly at high flow rate. The loss at the guide vane passage and runner passage exists relatively to a large extent. The loss at the guide vane passage reduces with increasing the flow rate. However, the loss at the runner passage is insensitive to the flow rate. Minimum amount of loss exists at the design flow rate. However, the loss increases rapidly at the off design flow rates. Especially at the partial flow rate, the loss at draft tube exists in a significant amount.

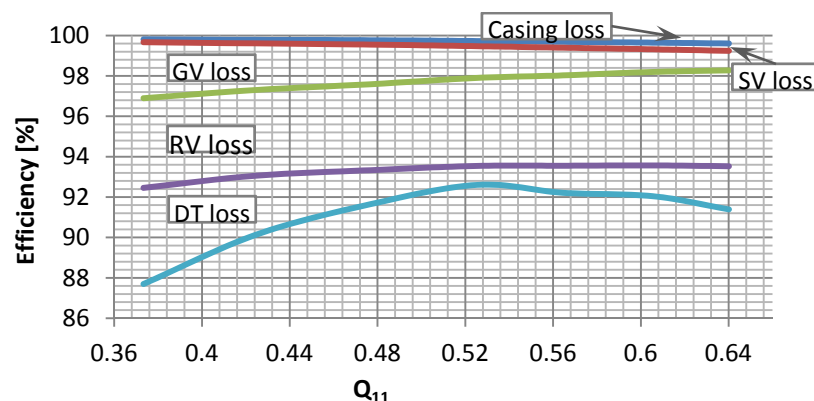


Figure 16. Component loss by the flow rate.

### 3.4. Fluid-Structure Interaction Analysis

In order to verify the runner blade structure integrity, fluid-structure interaction (FSI) is an effective method to calculate the stresses in the Francis turbine runner. Saeed *et al.* [17] found stress

maxima in different parts of the runner by FSI method. Xiao *et al.* [18] investigated the dynamic stresses in a Francis turbine runner successfully based on FSI analysis. In this study, the FSI analysis has been conducted for verifying the runner structure by the hydraulic force.

The material of SCS5 steel was applied for the runner, for which the tensile ultimate strength is 540 MPa and yield stress is 415 MPa. The pressure load applied on the runner surface is imported from the full domain CFD analysis at the design flow rate, where the flow rate is  $1.21 \text{ m}^3/\text{s}$  and turbine rotational speed is  $914 \text{ min}^{-1}$ .

The surfaces of hub, shroud, pressure and suction sides of the runner blades are selected for pressure loading as shown in Figure 17. The pressure imported to the runner surfaces for the FSI analysis is shown in Figure 18. The highest imported pressure of around 0.39 MPa exists on the hub and shroud surface near the runner inlet.

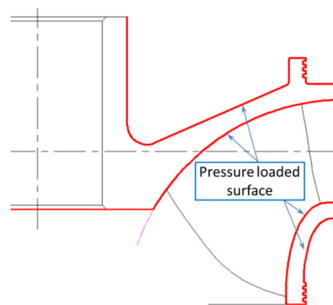


Figure 17. Runner hub and shroud surfaces for pressure loading.

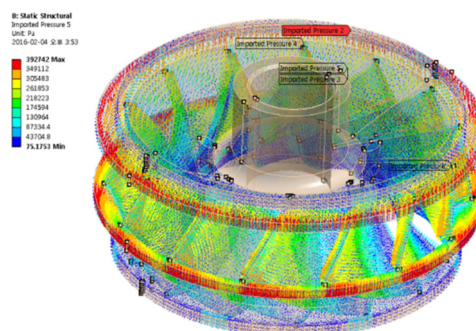


Figure 18. Pressure imported to the runner surfaces.

The structural feasibility is based on the stress on the runner, which is shown in Figure 19. The maximum stress point of 23 MPa can be found at the corner between runner blade leading edge and shroud, which is much lower than the material yield stress. The safety factor is 18, which is more than sufficient for a safe structure.

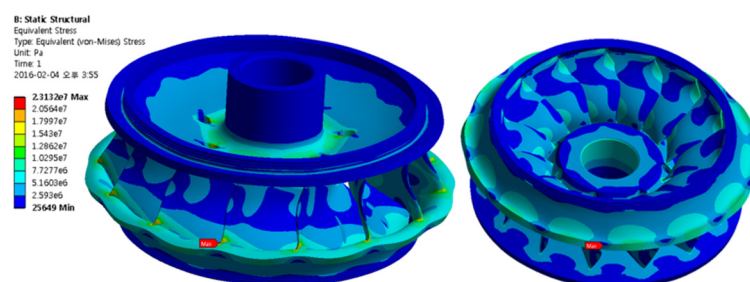


Figure 19. Stress distribution on the runner.

#### 4. Conclusions

The Francis turbine runner design and numerical analysis are presented for the Miryang power station of Korea. A successful design of the Francis turbine runner based on the one-dimension loss analysis and port area of the runner flow passage has been presented. The port area of runner blade plays a role of correcting the outflow angle from runner passage to reduce the swirl flow and the loss in the draft tube. Finally, the best efficiency of 92.6% is achieved by full domain calculation with leakage loss at the design point. From the FSI results it is evident that the maximum stress on the runner is much less than the ultimate stress the runner can withstand before failure.

**Acknowledgments:** This work was supported by the New and Renewable Energy of the Korea Institute of Energy Technology Evaluation and Planning (KETEP) grant funded by the Korea Government Ministry of Trade, Industry and Energy (No. 2013T100200079). Moreover, the authors are very grateful to Kazuyoshi Miyagawa of Waseda University, Japan, for his valuable advices.

**Author Contributions:** Zhenmu Chen conceived, designed and analyzed the hydro Francis turbine; Patrick M. Singh analyzed the data; Young-Do Choi planed the study project, as well as contributed the design and analysis tools; Zhenmu Chen and Patrick M. Singh wrote the paper and Young-Do Choi revised the paper.

**Conflicts of Interest:** The authors declare no conflict of interest.

#### Nomenclature

$\Delta p_{\text{total}}$	Total pressure difference
$a_0$	Guide vane opening
$a_r$	Port area
$B_g$	Guide vane height
$D_{r1}$	Runner inlet diameter
$g$	Gravitational acceleration
$H_e$	Effective head
$H_{gv}$	Guide vane head loss
$H_{\text{loss}}$	Pressure loss
$H_{\text{loss runner}}$	Runner pressure loss
$H_{\text{th}}$	Euler head
$m$	Hydraulic radius
$N$	Rotational speed
$N_s$	Specific speed
$p$	Pressure
$Q$	Flow rate
$Q_{11}$	Unit flow rate
$T$	Torque
$U$	Peripheral velocity
$V_{\text{th}}$	Velocity
$V_u$	Rotational component of absolute velocity
$W$	Relative velocity
$Z_g$	Guide vane number
$\alpha$	Flow angle
$\beta$	Relative flow angle
$\beta_b$	Blade angle
$\zeta$	Pressure loss coefficient
$\rho$	Water density
$\omega$	Angular speed

## Abbreviations

DT	Draft tube
GV	Guide vane
RV	Runner vane
SV	Stay vane

## References

1. Choi, G.W. *K-Water 2014 Sustainability Report*; K-Water: Deajeon, Korea, 2014.
2. Krishna, H.R. *Hydraulic Design of Hydraulic Machinery*; Ashgate Publishing Limited: Aldershot Hants, UK, 1997.
3. Laughton, M.A.; Warne, D.F. *Electrical Engineer's Reference Book*; George Newnes Ltd.: Oxford, UK, 2003.
4. Wei, Q.; Zhu, B.; Choi, Y.D. Internal Flow Characteristics in the Draft Tube of a Francis Turbine. *J. Korean Soc. Mar. Eng.* **2012**, *36*, 618–626. [[CrossRef](#)]
5. Wei, Q.; Choi, Y.D. The Influence of Guide Vane Opening on the Internal Flow of a Francis Turbine. *J. Korean Soc. Mar. Eng.* **2013**, *37*, 274–281. [[CrossRef](#)]
6. Ariff, M.; Salim, S.M.; Cheah, S.C. Wall  $Y^+$  Approach for Dealing with Turbulent Flow over a Surface Mounted Cube: Part 1—Low Reynolds Number. In Proceedings of the 7th International Conference on CFD in the Minerals and Process Industries, Melbourne, Australia, 9–11 December 2009.
7. Ariff, M.; Salim, S.M.; Cheah, S.C. Wall  $Y^+$  Approach for Dealing with Turbulent Flow over a Surface Mounted Cube: Part 2—High Reynolds Number. In Proceedings of the 7th International Conference on CFD in the Minerals and Process Industries, Melbourne, Australia, 9–11 December 2009.
8. Nechleba, M. *Hydraulic Turbine: Their Design and Equipment*; Artia: Prague, Czechoslovakia, 1957.
9. Mei, Z.Y. *Mechanical Design and Manufacturing of Hydraulic Machinery*; Avebury Technical: Hants, UK, 1991.
10. Ingram, G. *Basic Concepts in Turbomachinery*; Bookboon: London, UK, 2009.
11. Gorla, R.S.R.; Khan, A.A. *Turbomachinery: Design and Theory*; Marcel Dekker: New York, NY, USA, 2003.
12. Wu, J.; Shimmei, K.; Tani, K.; Niikura, K.; Sato, J. CFD-Based Design Optimization for Hydro Turbines. *J. Fluids Eng.* **2007**, *129*, 159–168. [[CrossRef](#)]
13. Alnaga, A.; Kueny, J.L. Optimal Design of Hydraulic Turbine Distributor. *WSEAS Trans. Fluid Mech.* **2008**, *2*, 175–185.
14. Shukla, M.K.; Jain, R. CFD Analysis of 3-D Flow for Francis Turbine. *Int. J. Mech. Eng.* **2011**, *2*, 93–100.
15. Navthar, R.R.; Tejas, J.; Saurabh, D.; Nitish, D.; Anand, A. CFD Analysis of Francis Turbine. *Int. J. Eng. Sci. Technol.* **2012**, *4*, 3194–3199.
16. ANSYS Inc. "ANSYS CFX Documentation" Ver. 12, 2012. Available online: <http://www.ansys.com> (accessed on 1 May 2013).
17. Saeed, R.A.; Galybin, A.N.; Popov, V. Modeling of Flow-Induced Stresses in a Francis Turbine Runner. *Adv. Eng. Softw.* **2010**, *41*, 1245–1255. [[CrossRef](#)]
18. Xiao, R.; Wang, Z.; Luo, Y. Dynamic Stresses in a Francis turbine Runner Based on Fluid-Structure Interaction Analysis. *Tsinghua Sci. Technol.* **2008**, *13*, 587–592. [[CrossRef](#)]



© 2016 by the authors; licensee MDPI, Basel, Switzerland. This article is an open access article distributed under the terms and conditions of the Creative Commons by Attribution (CC-BY) license (<http://creativecommons.org/licenses/by/4.0/>).